International Journal of Thermofluid Science and Technology (2019)
Vol. 6, No. 4, Paper No. 19060401
https://doi.org/10.36963/IJTST.19060401
Research Article

Influence of non-uniform heat source/sink and variable viscosity on mixed convection flow of third grade nanofluid over an inclined stretched Riga plate

M K Nayak[1], A K Abdul Hakeem[2], B Ganga[3]

[1]*Department of Physics, IHSE, Siksha "O" Anusandhan Deemed to be University, Bhubaneswar-751003, Odisha, India*
[2,3]*Department of Mathematics, Sri Ramakrishna Mission Vidyalaya College of Arts and Science, Coimbatore - 641020, India*

Received: 10 May 2019; Received in revised form: 8 August 2019; Accepted: 1 October 2019;
Published online 20 November 2019

Abstract

The present study focuses on the impact of non-uniform heat source/sink and temperature dependent viscosity modeled by Reynolds on Cattaneo-Christov heat flow of third grade nanofluid subject to an inclined stretched Riga plate. Fourth order R-K and shooting methods have been implemented to obtain the numerical solution of the transformed boundary layer equations. The achievability of the present study is that the material constants associated with third grade fluid augment the fluid motion and boils down the fluid temperature leading to ascending velocity boundary layer and descending thermal boundary layer. And viscosity parameter enhances the heat transfer rate from the plate. Furthermore, augmented space and temperature dependent heat source upsurges the fluid temperature and the related thermal boundary layer thickness.

Keywords: Non-uniform heat source/sink; Reynolds variable viscosity model; Cattaneo-Christov heat flux model; Third-grade nanofluid; Inclined stretched Riga plate.

1. Introduction

It was the time when the World was looking forward to greater research contributions from across the Globe; Choi et al. [1] played an important role in discovering experimentally the concept of nanofluids. Nanofluids are the novel type fluids that contain nanoparticles, such as metals, oxides, carbides, and nitrides, with sizes less than 100 nm have higher thermal conductivity compared to that of the conventional base fluid, such as water, engine oil, and

Corresponding e-mail: mkn2122@gmail.com (M. K. Nayak)

ethylene. Such extraordinary characteristics of nanofluids (fluids with more heat transfer capability) make them potentially useful to serve as better coolant in nuclear reactor, micro manufacturing, refrigeration, automotives, heat exchangers, aircrafts and space applications and other high energy devices, antibacterial treatment, wound treatment, asthma treatment, targeted drug release/drug delivery [2-22].

Nomenclature

(u,v)	velocity components in (x, y) directions	τ_w	wall shear stress
CCHF	Catteneo-Christov heat flow	*TGNF*	Thirdgrade nanofluid
TBL	thermal boundary layer	CBL	concentration boundary layer
HTR	heat transfer rate	λ	relaxation time
$(\Omega_1^*,\Omega_2^*,\Omega_3^*)$	material constants	υ_f	kinematic viscosity
(T,C)	fluid(temperature, concentration)	k_f	thermal conductivity
(T_∞,C_∞)	ambient (temperature, concentration)	ρ_f	density of fluid
$f(\eta)$	dimensionless stream function	j_0	current density
(λ_T,λ_C)	(thermal, solutal) buoyancy parameters	$U_w(x)$	stretching velocity of the plate
p	width of magnets and electrodes	Υ	Deborah number expansion
(β_T,β_C)	volumetric coefficient of (thermal, mass)		
g	gravitational acceleration	δ	width parameter
M_0	magnetization of permanent magnets	q	heat flux
Q_0	coefficient of space dependent heat source/sink		
$\alpha_f=\frac{k_f}{(\rho C_p)_f}$	thermal diffusivity		
Q_1	coefficient of temperature dependent heat source/sink		
$\tau=(\rho C_p)_p/(\rho C_p)_f$	heat capacity ratio	V	velocity
$(\Omega_1,\Omega_2,\Omega_3)$	non-dimensional material constants	ε	velocity ratio parameter
Nb	Brownian motion parameter	*Nt*	thermophoresis parameter,
Re_x	local Reynolds numbers	Λ	angle with vertical direction
D_B	Brownian diffusion coefficient	D_T	thermophoretic diffusion coefficient
C_p	specific heat at constant pressure	$U_w(x)=ax$	stretching velocity
η	non-dimensional vertical distance	m	Reynolds model viscosity parameter
P_r	Prandtl number	μ_0	reference viscosity
Le	Lewis number	Γ	modified Hartmann number
q_w	wall heat flux	J_m	wall mass flux
Subscripts			
f	fluid	s	surface

w	quantities at wall	∞	quantities at free stream

Looking at the Riga-plate arrangement it produces a Lorentz force of exponentially decaying nature which induces the flow over the plate. Pantokratoras and Magyari [23] were the pioneers to study electro-magnetohydrodynamic flow over a horizontal Riga plate. Later, Ahmad et al. [24] studied the flow of nanofluid past a Riga plate considering the influence of nanoparticles size on skin friction. Hakeem et al. [25] investigated the impact of exponentially variable viscosity and permeability on Blasius flow of Carreu nanofluid over an electromagnetic plate.

In fact, third grade fluid imparts features such as normal stresses and shear thinning/shear thickening phenomena. Examples of such fluids are molten plastics, slurry flows, highly viscous silicon oils and dilute polymer solutions and many more. Hayat et al. [26] explored in their investigation that velocity field disparages with enhancing of melting parameter and reducing wall thickness parameter. The deviations of flow variables for third-grade fluid are significant compared to the Newtonian fluid flow (Ready et al. [27]).

The interesting aspect of CCHF model is that thermal relaxation was added to Fourier's law by Cattaneo [28]. The Cattaneo's model was further improved by Christov [29] after which this model is known as CCHF model. Augmentation in thermal relaxation time contributes to low temperature (Imtiaz et al. [30]). Hayat and Nadeem [31] declared in their study that the heat source/sink that exerts strong influence on HTR associated with the TBL. Heat source/sink alters the HTR and thereby changes the structure of TBL. The fluid temperature and wall shear stress increase due to increase in heat source/sink parameter in stagnation point flow past stretching sheet (Sharma et al. [32]).

In brief, the present study is clearly meant for exploring the effects of non-uniform heat source/sink and temperature dependent variable viscosity on the flow of third grade nanofluid flow over an inclined Riga plate. Further, CCHF model is invoked to obtain the behavior of relaxation time. An appropriate numerical solution of the developed similarity transferred coupled non-linear differential equations has been devised by using fourth order R-K method through shooting technique. The influence of various significant emerging parameters concerned presented through appropriate graphs and discussion.

2. Formulation of the problem

In the current study, we consider the steady incompressible flow of third grade nanofluid over an inclined stretched Riga-plate. A Cartesian coordinate system is chosen such that x-axis is along the plate and y-axis is normal to it (Fig.1). The plate is stretched by equal and opposite forces with velocity $U_w(x) = ax$. Electromagnetic field of the Riga-plate induces an exponentially descending Lorentz force parallel to the plate surface.

The equations of continuity, momentum and energy governing the flow of third grade nanofluid in the presence of non-uniform heat source/sink are [8, 14, 26, 31]:

$$\frac{\partial u}{\partial x}+\frac{\partial v}{\partial y}=0 \tag{1}$$

$$u\frac{\partial u}{\partial x}+v\frac{\partial u}{\partial y}=\frac{1}{\rho_f}\frac{\partial}{\partial y}\left(\mu_f\frac{\partial u}{\partial y}\right)+\frac{\Omega_1^*}{\rho_f}\left(u\frac{\partial^3 u}{\partial x\partial y^2}+\frac{\partial u}{\partial x}\frac{\partial^2 u}{\partial y^2}+3\frac{\partial u}{\partial y}\frac{\partial^2 u}{\partial x\partial y}+v\frac{\partial^3 u}{\partial y^3}\right)$$
$$+\frac{2\Omega_2^*}{\rho_f}\frac{\partial u}{\partial y}\frac{\partial^2 u}{\partial x\partial y}+\frac{6\Omega_3^*}{\rho_f}\left(\frac{\partial u}{\partial y}\right)^2\left(\frac{\partial^2 u}{\partial y^2}\right) \tag{2}$$
$$+g\beta_T\left(T-T_\infty\right)\cos\Lambda+g\beta_C\left(C-C_\infty\right)\cos\Lambda+\frac{\langle\vec{F}\rangle}{\rho}$$

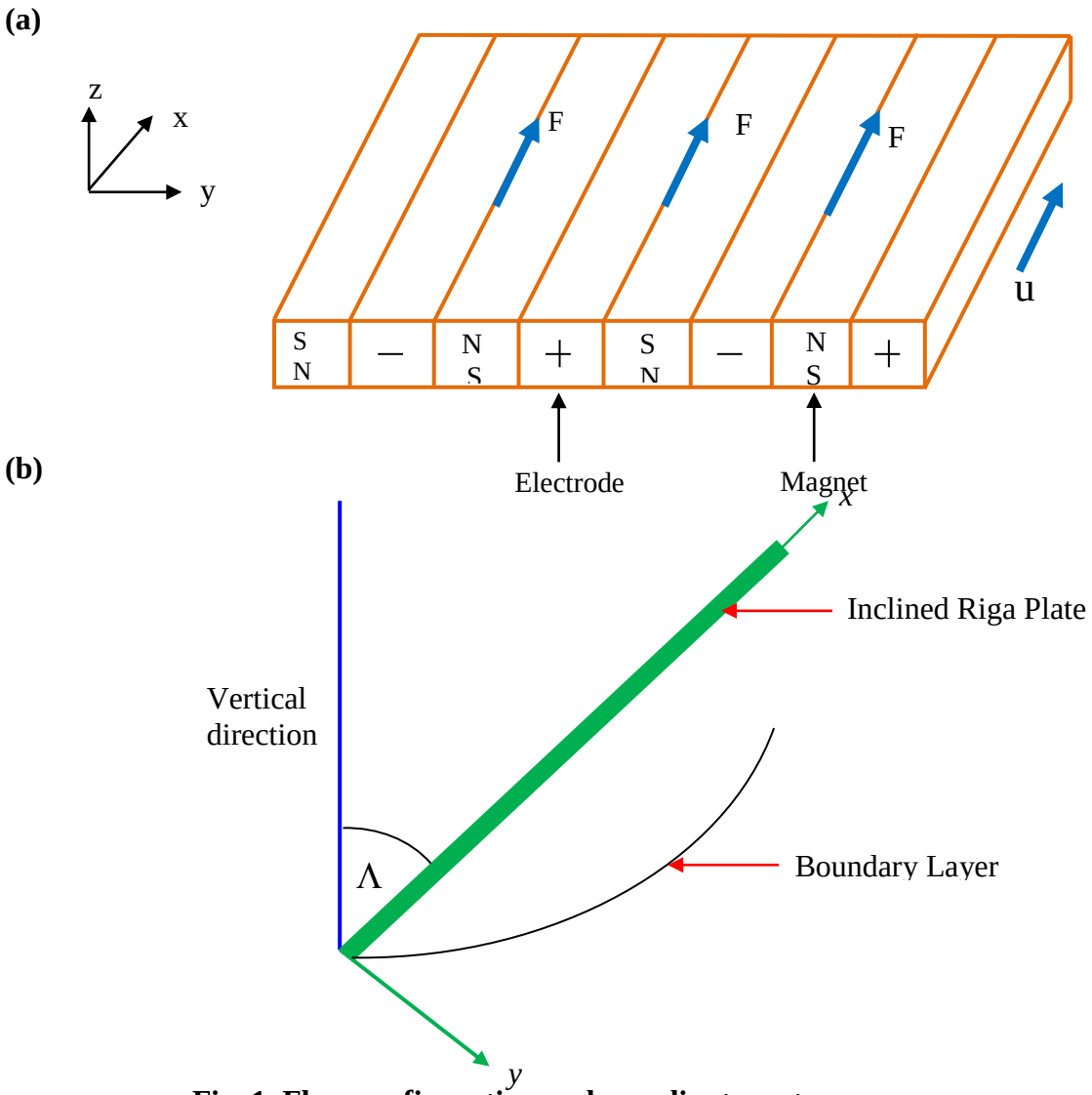

Fig. 1. Flow configuration and coordinate system.

$$u\frac{\partial T}{\partial x}+v\frac{\partial T}{\partial y}=-\frac{\nabla.q}{\left(\rho C_p\right)_f}+\tau\left[D_B\frac{\partial C}{\partial y}\frac{\partial T}{\partial y}+\frac{D_T}{T_\infty}\left(\frac{\partial T}{\partial y}\right)^2\right]+\frac{q'''}{\left(\rho C_p\right)_f} \tag{3}$$

$$u\frac{\partial C}{\partial x}+v\frac{\partial C}{\partial y}=D_B\frac{\partial^2 C}{\partial y^2}+\frac{D_T}{T_\infty}\frac{\partial^2 T}{\partial y^2} \tag{4}$$

According to CCHF theory, we reveal [13]:

$$q+\lambda\left[\frac{\partial q}{\partial t}+V.\nabla q-q.\nabla V+\left(\nabla.V\right)q\right]=-k_f\nabla T \tag{5}$$

where λ is the relaxation time of heat flux/thermal relaxation of the fluid, V is the velocity vector and q is the heat flux. It is the time taken for the shear stress in a viscoelastic material to reduce $1/e$ of its initial value.

Setting $\lambda=0$ in eq (5), classical Fourier's law can be obtained. Considering the flow as steady $\left(\frac{\partial q}{\partial t}=0\right)$ and incompressible $\left(\nabla.V=0\right)$, eq (5) takes the form

$$q+\lambda\left(V.\nabla q-q.\nabla V\right)=-k\nabla T \tag{6}$$

The energy equation then becomes

$$\begin{aligned}u\frac{\partial T}{\partial x}+v\frac{\partial T}{\partial y}+\lambda\left(u\frac{\partial u}{\partial x}\frac{\partial T}{\partial x}+v\frac{\partial v}{\partial y}\frac{\partial T}{\partial y}+u\frac{\partial v}{\partial x}\frac{\partial T}{\partial y}+v\frac{\partial u}{\partial y}\frac{\partial T}{\partial x}+2uv\frac{\partial^2 T}{\partial x\partial y}+u^2\frac{\partial^2 T}{\partial x^2}+v^2\frac{\partial^2 T}{\partial y^2}\right)\\ =\alpha_f\left(\frac{\partial^2 T}{\partial y^2}\right)+\tau\left[D_B\frac{\partial C}{\partial y}\frac{\partial T}{\partial y}+\frac{D_T}{T_\infty}\left(\frac{\partial T}{\partial y}\right)^2\right]+\frac{q'''}{\left(\rho C_p\right)_f}\end{aligned} \tag{7}$$

According to Grinberg [33], the force density averaged over the span wise coordinate z takes the form

$$\langle\vec{F}\rangle=\frac{\pi}{8}j_0M_0e^{-\left(\frac{\pi}{p}\right)y}$$

Hence, $\frac{\langle\vec{F}\rangle}{\rho_f}=\frac{\pi j_0M_0}{8\rho_f}e^{-\left(\frac{\pi}{p}\right)y}$ is the Grinberg term of the momentum equation (2) which does not depend upon the flow velocity.

The requisite boundary conditions are :

$$\left.\begin{aligned}&u=U_w\left(x\right)=ax,\ v=0,\ T=T_w,\ C=C_w \quad at \quad y=0\\ &u\to U_\infty\left(x\right),\quad T\to T_\infty,\quad C\to C_\infty \qquad as \quad y\to\infty\end{aligned}\right\} \tag{8}$$

The non-uniform heat sourc/sink is expressed as

$$q''' = \frac{k_f U_w}{x\upsilon_f}\left[Q_0\left(T - T_\infty\right)e^{-\eta} + Q_1\left(T - T_\infty\right)\right] \tag{9}$$

Where Q_0 and Q_1 are the coefficients of space and temperature dependent heat source/sink respectively. The case $Q_0 > 0$ and $Q_1 > 0$ contributing internal heat generation while $Q_0 < 0$ and $Q_1 < 0$ contribute internal heat absorption.

The suitable transformations employed for the purpose are :

$$\left.\begin{aligned} &\psi = \sqrt{Ux\upsilon_f}\ f\left(\eta\right), u = axf'\left(\eta\right),\ v = -\sqrt{a\upsilon_f}\ f\left(\eta\right), \\ &\theta\left(\eta\right) = \frac{T - T_\infty}{T_w - T_\infty},\ \phi\left(\eta\right) = \frac{C - C_\infty}{C_w - C_\infty},\ \eta = \sqrt{\frac{U}{\upsilon_f x}}\, y \end{aligned}\right\} \tag{10}$$

Where $U = U_w + U_\infty$ is the composite velocity. The incompressibility condition is satisfied.

According to Reynolds model, the expression for temperature dependent viscosity is

$$\mu_f\left(\theta\right) = \mu_0 e^{-m\theta} \tag{11}$$

which can be expressed as

$$\mu_f\left(\theta\right) = \mu_0\left[1 - \left(m\theta\right) + o\left(m^2\right)\right] \tag{12}$$

With the help of eqs (9), (10) and (12) and neglecting higher order terms in eq. (12) and using the resulting expression, eqs (2), (4), (7) and (8) take the form:

$$\begin{aligned} \left(1 - m\theta\right)f''' - m\theta' f'' - \left(f'\right)^2 + ff'' + \frac{1}{\left(1 - m\theta\right)}\left[\begin{array}{r} \Omega_1\left(2ff''' - ff^{iv}\right) + \left(3\Omega_1 + 2\Omega_2\right)\left(f''\right)^2 \\ + 6\Omega_3\,\mathrm{Re}\, f'''\left(f''\right)^2 \end{array}\right] \\ + \lambda_T\theta\cos\Lambda + \lambda_C\phi\cos\Lambda + \Gamma e^{-\delta\eta} = 0 \end{aligned} \tag{13}$$

$$\theta'' + \mathrm{Pr}\left[f\theta' - \Upsilon\left(ff'\theta' + f^2\theta''\right) + N_b\theta'\phi' + N_t\left(\theta'\right)^2\right] + \left(Q_0 e^{-\eta} + Q_1\theta\right) = 0 \tag{14}$$

$$\phi'' + Le\,\mathrm{Pr}\, f\phi' + \left(\frac{N_t}{N_b}\right)\theta'' = 0 \tag{15}$$

with

$$\left.\begin{aligned} &f'\left(0\right) = 1,\ f\left(0\right) = 0, \theta\left(0\right) = 1, \phi\left(0\right) = 1\ \ at\ \eta = 0 \\ &f' \to 1 - \varepsilon,\ \theta \to 0,\ \ \phi \to 0 \quad\ \ as\ \ \eta \to \infty \end{aligned}\right\} \tag{16}$$

where

$$\left.\begin{aligned}
&\Omega_1=\frac{a\Omega_1^*}{\mu_0},\ \Omega_2=\frac{a\Omega_2^*}{\mu_0},\ \Omega_3=\frac{a\Omega_3^*}{\mu_0},\ \Gamma=\frac{\pi j_0 M_0}{8aU\rho_f},\ \lambda_T=\frac{g\beta_T\left(T_w-T_\infty\right)}{xU},\\
&\lambda_C=\frac{g\beta_C\left(C_w-C_\infty\right)}{xU},\ \mathrm{Re}=\frac{ax^2}{\upsilon_f},\ \delta=\frac{\pi}{a\sqrt{\frac{U}{x\upsilon_f}}},\ P_r=\frac{\upsilon_f}{\alpha_f},\ \ \Upsilon=a\lambda,\upsilon_f=\frac{\mu_0}{\rho_f}\\
&N_b=\frac{\tau D_B\left(C_w-C_\infty\right)}{\upsilon_f},\ N_t=\frac{\tau D_T\left(T_w-T_\infty\right)}{T_\infty\upsilon_f},\ Le=\frac{\alpha_f}{D_B},\ \varepsilon=\frac{U_w}{U}
\end{aligned}\right\} \tag{17}$$

The local skin friction coefficient

$$C_f=\frac{2\tau_w}{\rho_f U_w^2} \tag{18}$$

Where $\tau_w=\left[\mu_f\frac{\partial u}{\partial y}+\Omega_1^*\left(u\frac{\partial^2 u}{\partial x\partial y}+\nu\frac{\partial^2 u}{\partial y^2}+2\frac{\partial u}{\partial x}\frac{\partial u}{\partial y}\right)+2\Omega_3^*\left(\frac{\partial u}{\partial y}\right)^3\right]_{y=0}$ denotes the wall shear stress.

The non-dimensional local skin friction coefficient

$$\mathrm{Re}^{\frac{1}{2}}C_f=f''(0)+\frac{\Omega_1}{(1-m\theta)}\left[3f'(0)f''(0)-f(0)f'''(0)\right]+\frac{\Omega_3}{(1-m\theta)}\left[f''(0)\right]^3 \tag{19}$$

$$Sh_x=\frac{x J_m}{D_B\left(C_w-C_\infty\right)} \tag{20}$$

with $J_m=-D_B\left(\frac{\partial C}{\partial y}\right)_{y=0}$ denotes the wall mass flux.

The non-dimensional local Sherwood number

$$Re^{-\frac{1}{2}}Sh_x=-\phi'(0) \tag{21}$$

3. Numerical Methodology

The system of equations (13) – (15) together with the equation (16) are solved by using 4th order RK method along with shooting technique. A relevant short logic diagram depicting the algorithm of the solution is mentioned below.

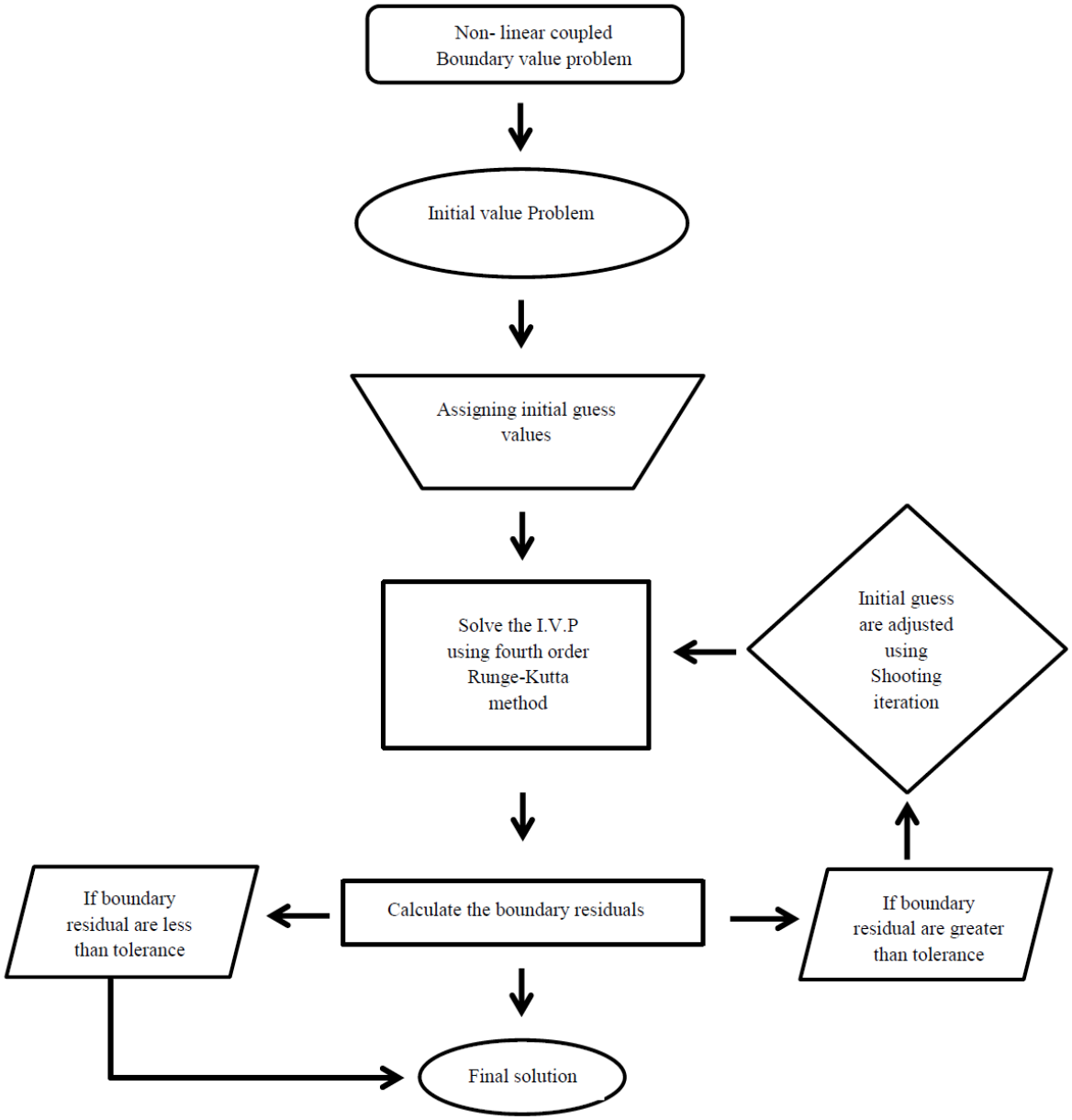
Non- linear coupled Boundary value problem
Initial value Problem
Assigning initial guess values
Solve the I.V.P using fourth order Runge-Kutta method
Initial guess are adjusted using Shooting iteration
Calculate the boundary residuals
If boundary residual are less than tolerance
If boundary residual are greater than tolerance
Final solution

4. Results and Discussion

The present study primarily focuses on the effect of non-uniform heat source/sink and variable viscosity on mixed convection CCHF of TGNF over an inclined stretched Riga plate. An appropriate numerical solution of the transformed governing equations is obtained. The values of the parameters considered for the present simulation are: $\Omega_1 = \Omega_2 = \Omega_3 = 0.1$, $\lambda_c = \lambda_T = 0.3$, $\Upsilon = 0.1$, $\Lambda = 45^\circ$, $m = 0.5$, $\delta = 0.2$, $\Gamma = 0.1$, $\varepsilon = 0.6$ $\mathrm{Pr} = 1$, $N_b = N_t = 0.5$, $Q_0 = Q_1 = 0.1$ and $Le = 0.5$. The present analysis imparts well exploration regarding the effects of different pertinent parameters on velocity, temperature, concentration, skin friction and Sherwood number profiles through suitable graphical representation and pretty discussion.

Figs. 2 and 3 bring to the focus the behavior of λ_T and λ_C on fluid velocity. It is noticed that an accelerated fluid motion takes place due to enhancement in λ_T and λ_C which in turn establishes thicker MBLs in the respective flow domains. Fig.4 reveals that an augmented m contributes to the accelerated fluid motion giving rise to the same environment that due to the presence of thermal and solutal buoyancies. The fundamental reason behind this ascending trend is that viscous force dominates over the inertial force. Increasing values of Γ yields the rising flow contributing to high wall velocity gradient (Fig.5). For the more and more the angle of inclination of the plate, VBL thickness gets reduced (Fig.6). As ε rises, the flow diverges from the plate towards the ambient fluid with gradually more descending trend (Fig.7). Figs. 8, 9 and 10 portray the influence of Ω_1, Ω_2 and Ω_3 on velocity profiles respectively. Fluid velocity gets diminution near the plate within the range $(0 \le \eta \le 0.5)$ and it shows a reverse trend followed by a transition at $\eta = 1.5$ under the impact of increasing Ω_1. Indeed, material parameters are inverse relation to viscosity. That is why increase in Ω_2 and Ω_3 belittles the fluid viscosity thereby favors the fluid motion.

It is obvious from Figs. 11, 12 and 13 that increase in Ω_1 and Ω_2 undermine the fluid temperature $\theta(\eta)$ while that of Ω_3 upsurges it. A unique feature of these $\theta(\eta)$ profiles is the appearance of non-linearity which is due to the presence of non-linear terms in governing energy equation. Fig.14 demonstrates the non-linear decaying nature of the $\theta(\eta)$ profiles due to increase in m leading to shrinking of TBL in the entire flow regime. A non-linear $\theta(\eta)$ profile due to distinguished behavior of Pr is visualized in Fig. 15. It is noticed here that increasing Pr makes the $\theta(\eta)$ less (due to low thermal diffusivity compared to viscosity) which in turn reduces TBL thickness. However, high Prandtl fluid $(\mathrm{Pr} = 6)$ exhibits slow response to such diminishing trend. Further, symmetrical diminishing trend of non-linear $\theta(\eta)$ profiles due to increase in Υ is envisioned in Fig.16. This is because of low temperature profile under the influence of CCHF

model. Figs. 17 and 18 offer the non-linear, however, increasing behavior of non-dimensional $\theta(\eta)$ due to enhancement in N_b and N_t respectively. The rationally behind this is that higher Brownian diffusion and thermophoresis force contribute to stronger fluid temperature. Behavior of non-dimensional $\theta(\eta)$ due to the influence of non-uniform heat source/sink $(Q_0 and\, Q_1)$ is reflected from Figs. 19 and 20 respectively. In other words, increase in Q_0 and Q_1 upsurge the $\theta(\eta)$ in non-linear fashion throughout the growing TBL associated with enhanced wall temperature gradient.

Figs. 21, 22 and 23 illustrate that hiked Ω_1 and Ω_2 upsurge the fluid concentration $\phi(\eta)$ while that of Ω_3 undermine it. Further, Fig. 24 indicates an increasing non-linear behavior of $\phi(\eta)$ due to rise in m generating ascending CBL. Fig. 25 displays that increase in Le belittles the $\phi(\eta)$ developing descending CBL. This is only due to lower mass diffusivity. Fluid concentration $\phi(\eta)$ profiles enhance in response to rise in N_b and N_t, however, enhancement is more in case of N_t (Fig. 26 and 27). This is due to the effective motion of nanoparticles from the plate to the fluid.

Variation of skin friction coefficient $\mathrm{Re}^{\frac{1}{2}} C_f$ against m for different Ω_1, Ω_2 and Ω_3 is shown in Fig.28. It is conveyed from this figure that $\mathrm{Re}^{\frac{1}{2}} C_f$ gets augmented due to increase in Ω_1 and Ω_2 while the wall shear stress shows diminution due to enhancement in Ω_3. Meanwhile, Fig. 29 provides the variation of the wall shear stress against m for different Γ and Λ. What is found here is that increase in Γ enhances the wall shear stress. As far as the behavior of Sherwood number $\mathrm{Re}^{-\frac{1}{2}} Sh_x$ is concerned, influence of Ω_1 and Ω_2 on it are diametrically opposite (Fig.30).

Augmented Ω_1 enhances the mass transfer rate from the plate while that of Ω_2 significantly reduces the same. Ascending trend of mass flux is prominent for comparatively higher Ω_1 $(\Omega_1 = 0.3)$.

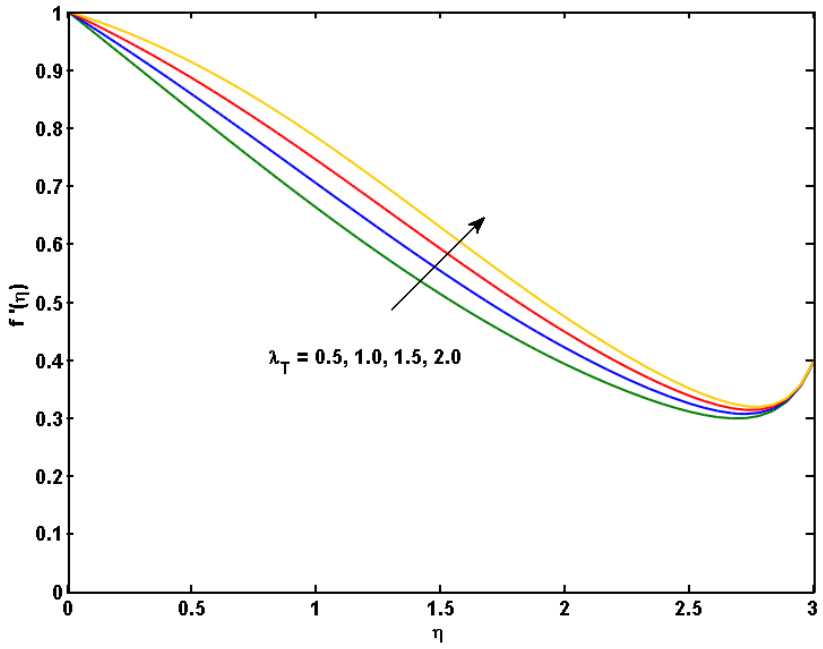

Fig.2 $f'(\eta) Vs\ \lambda_T$

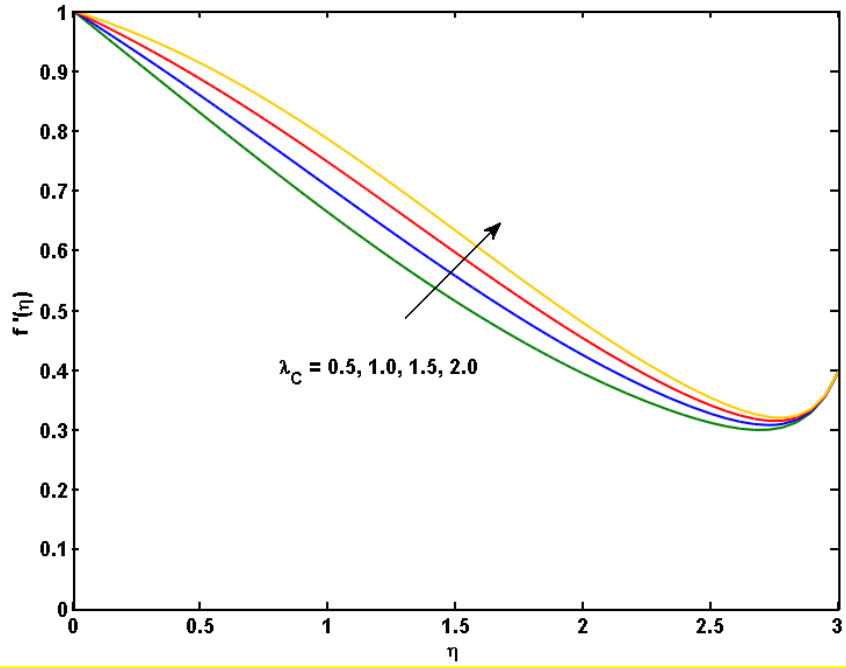

Fig.3 $f'(\eta) Vs\ \lambda_c$

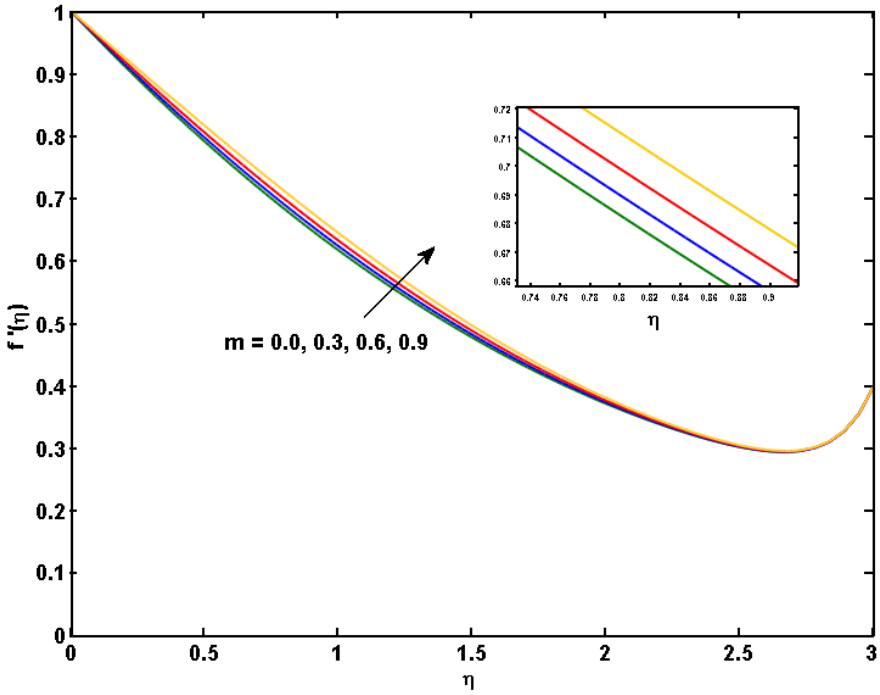

Fig. 4 $f'(\eta) Vs\ m$

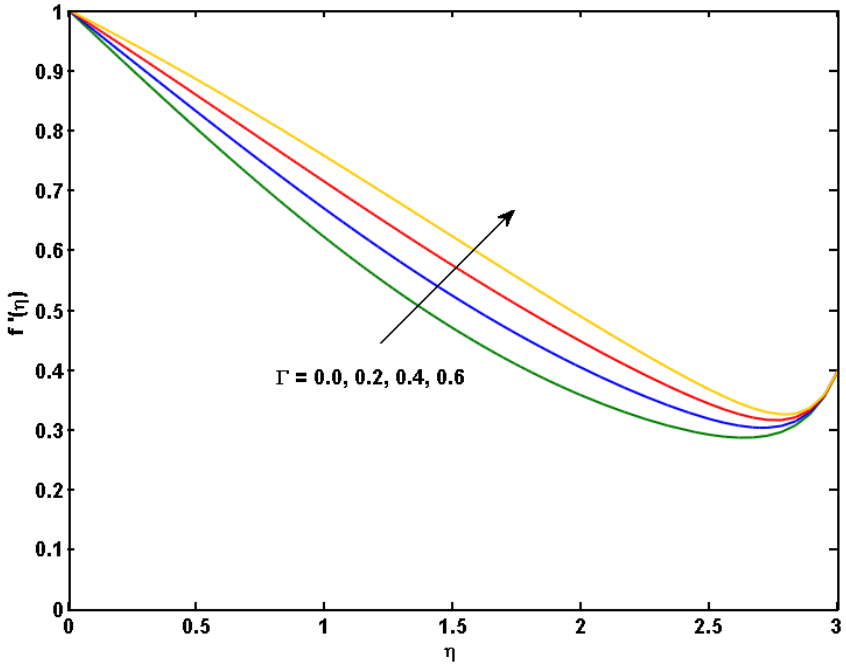

Fig. 5 $f'(\eta) Vs\ \Gamma$

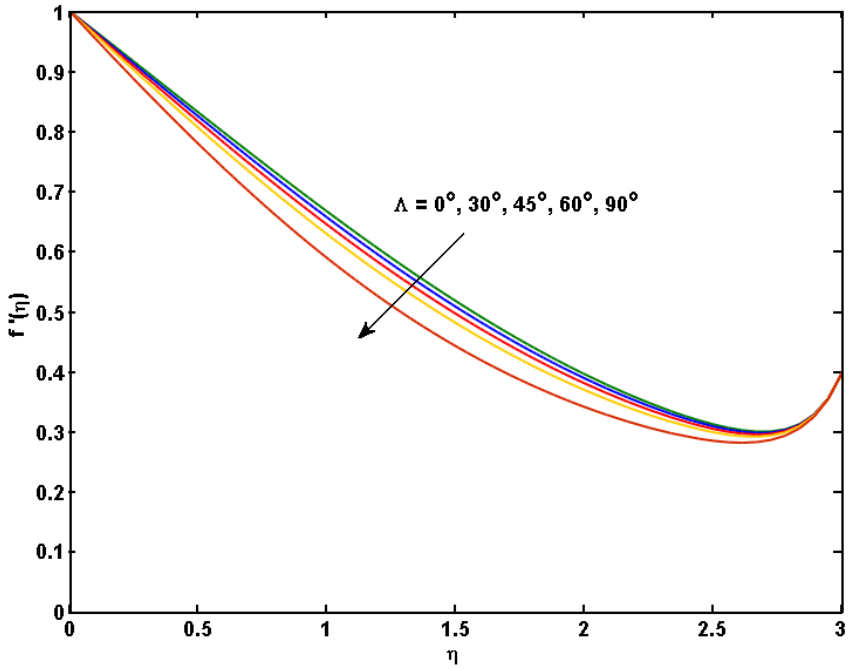

Fig. 6 $f'(\eta) Vs\ \Lambda$

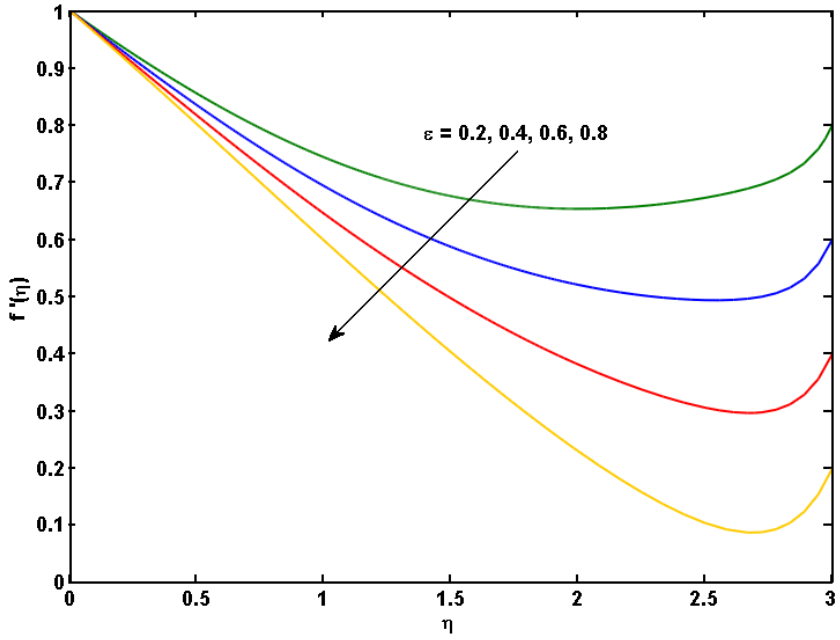

Fig. 7 $f'(\eta) Vs\ \varepsilon$

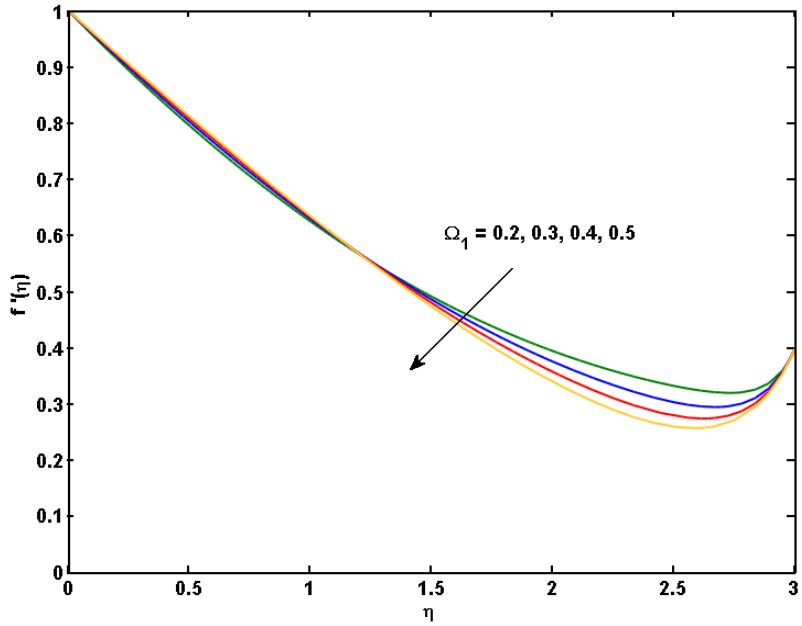

Fig. 8 $f'(\eta) Vs\ \Omega_1$

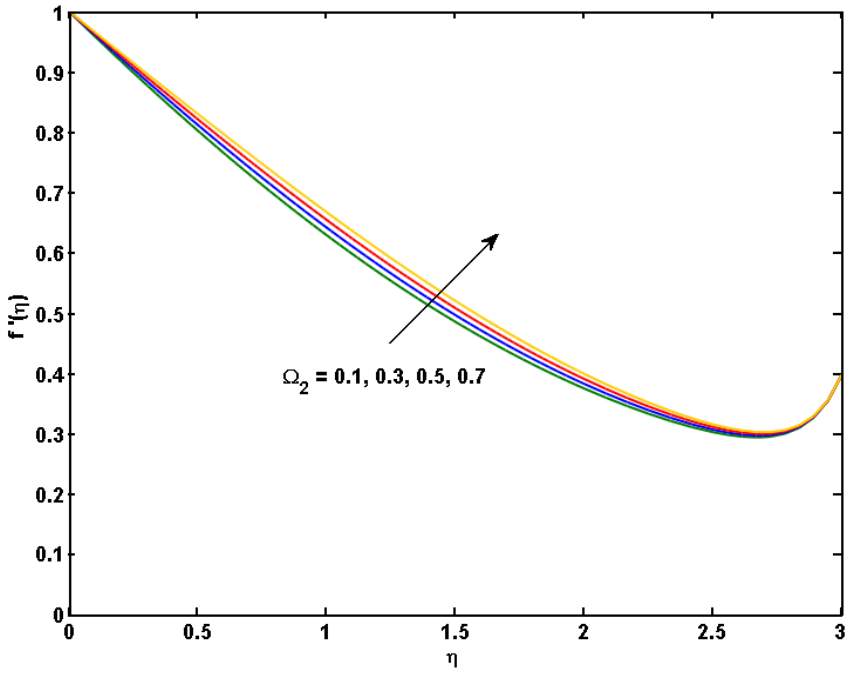

Fig. 9 $f'(\eta) Vs\ \Omega_2$

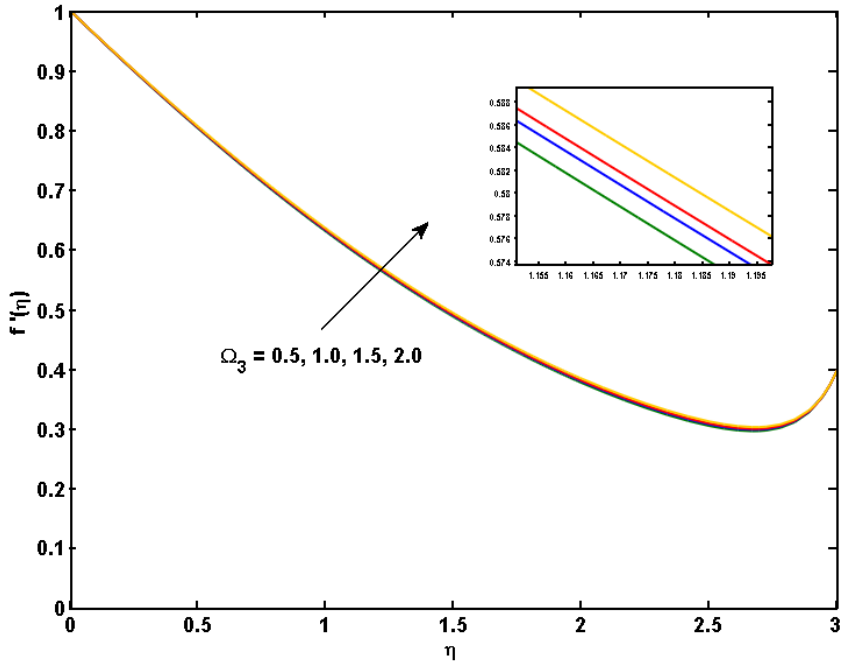

Fig.10 $f'(\eta) Vs\ \Omega_3$

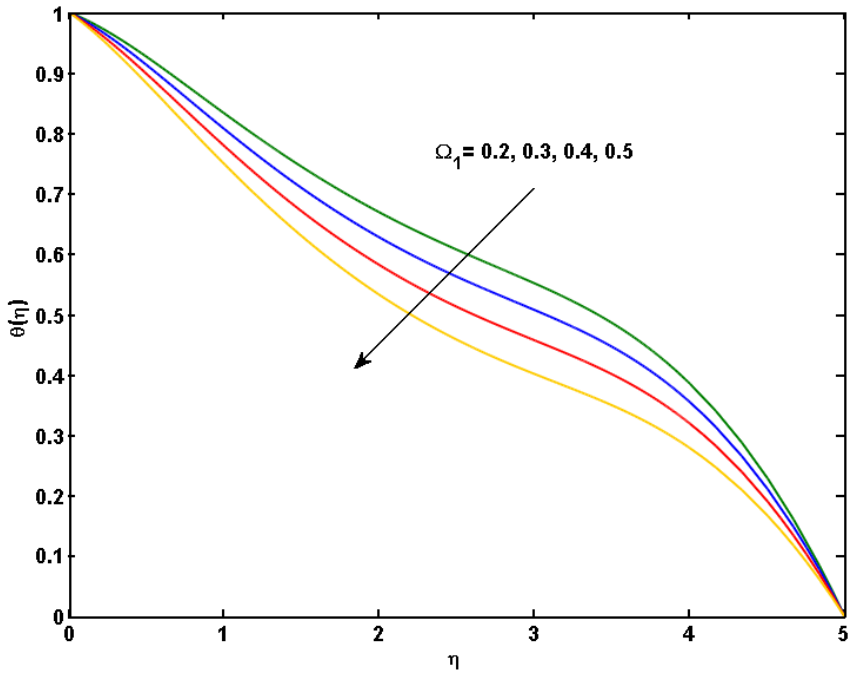

Fig.11. $\theta(\eta) Vs\ \ \Omega_1$

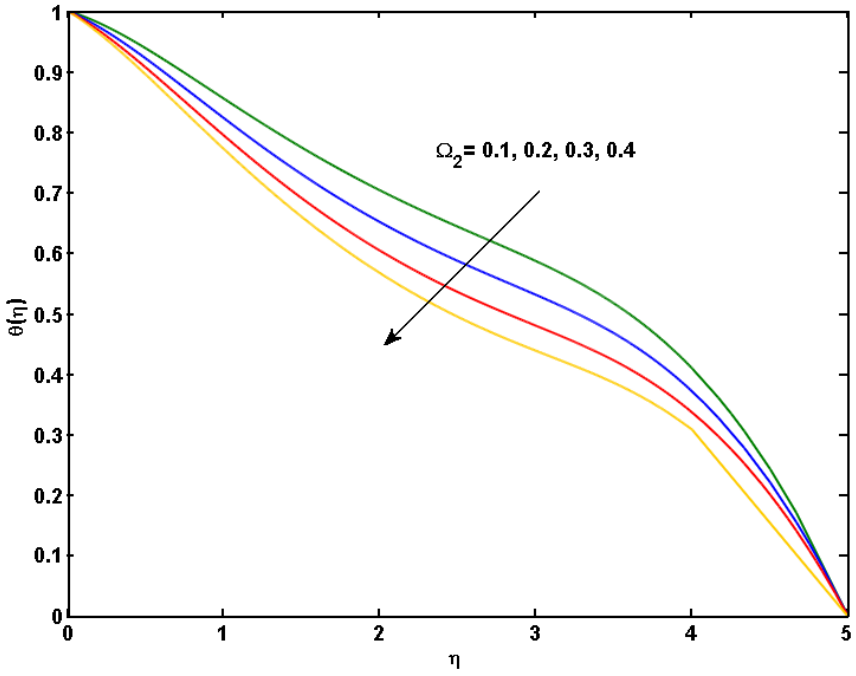

Fig.12 $\theta(\eta) Vs\ \ Q_2$

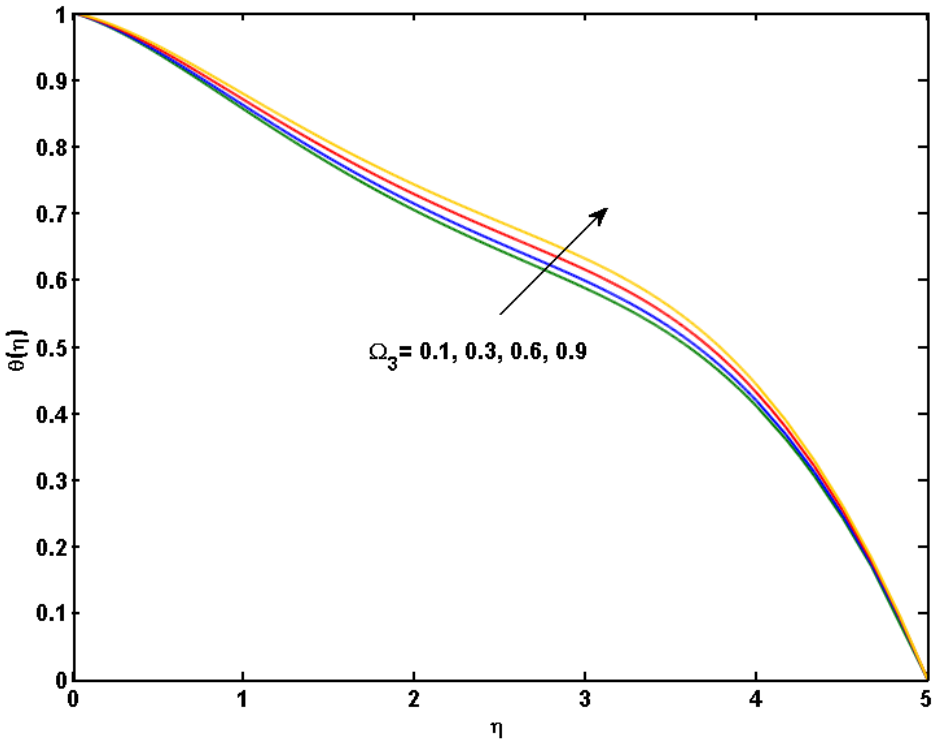

Fig.13 $\theta(\eta) Vs\ \ Q_3$

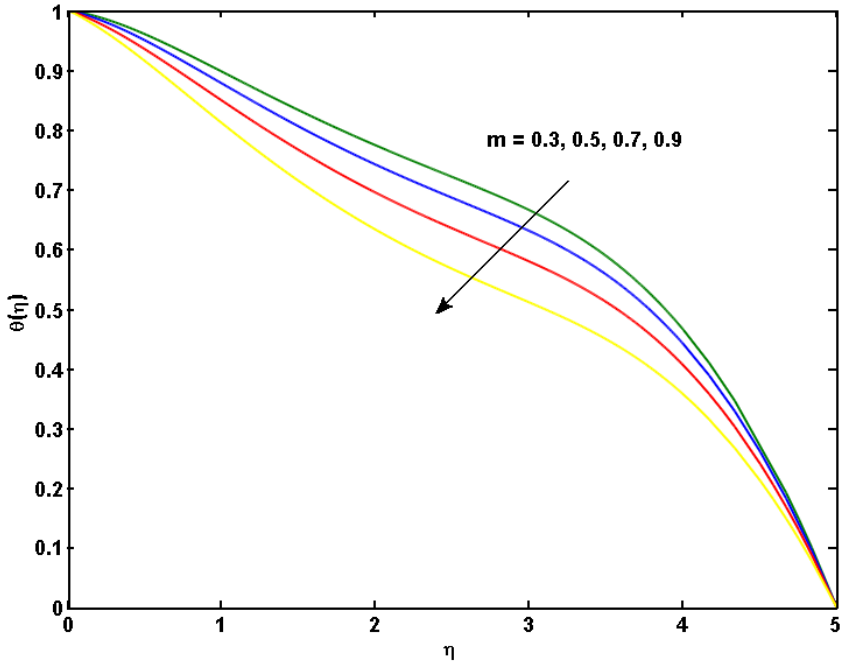

Fig.14 $\theta(\eta) Vs\ \ m$

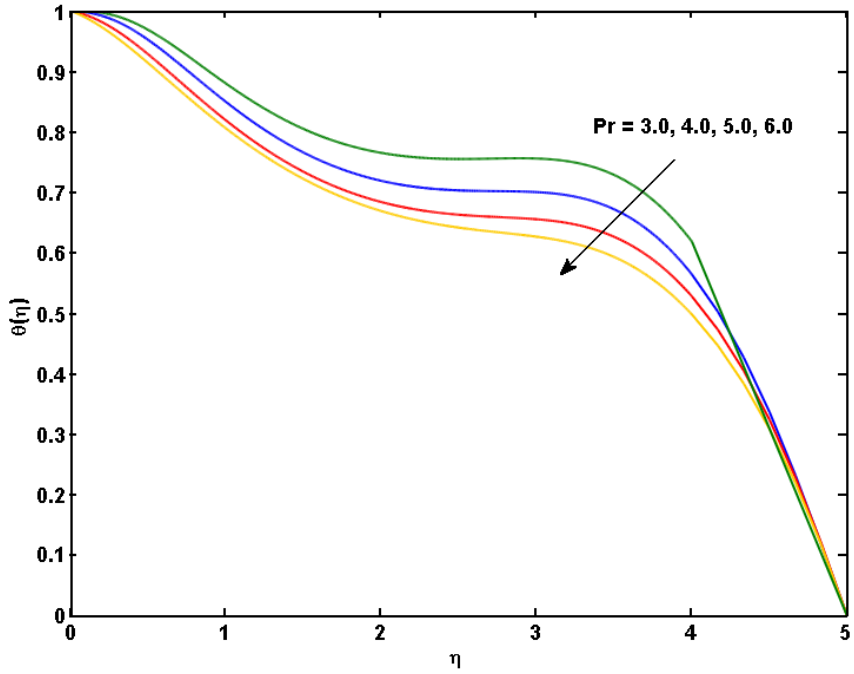

Fig.15 $\theta(\eta) Vs$ Pr

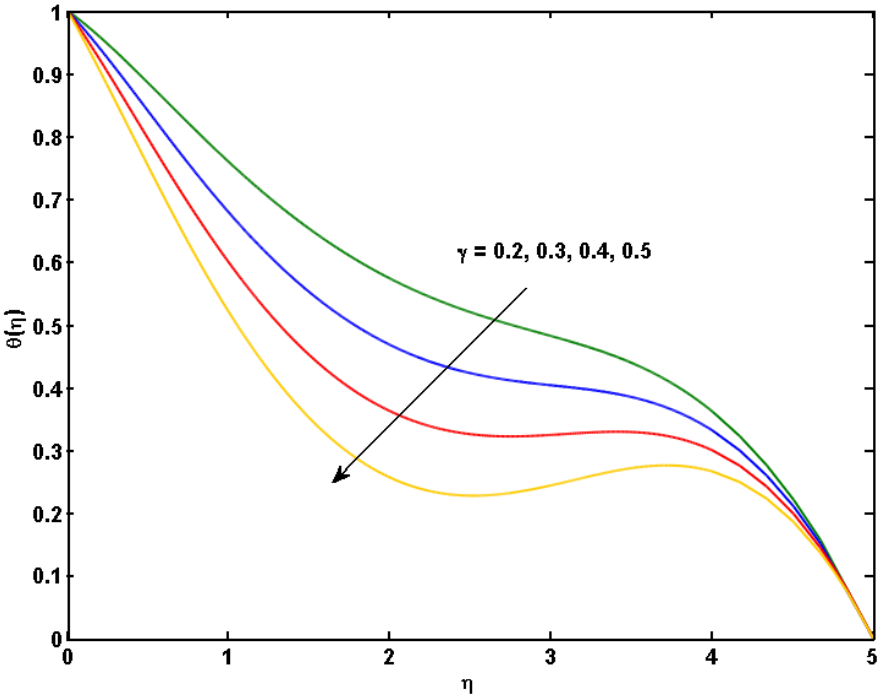

Fig.16 $\theta(\eta) Vs\ \Upsilon$

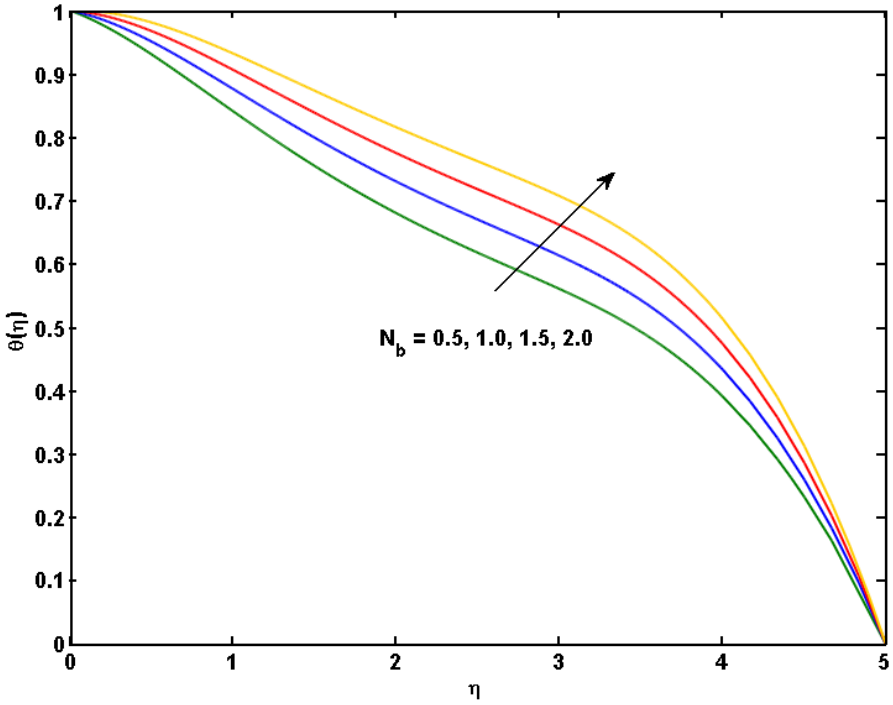

Fig.17 $\theta(\eta) Vs\ Nb$

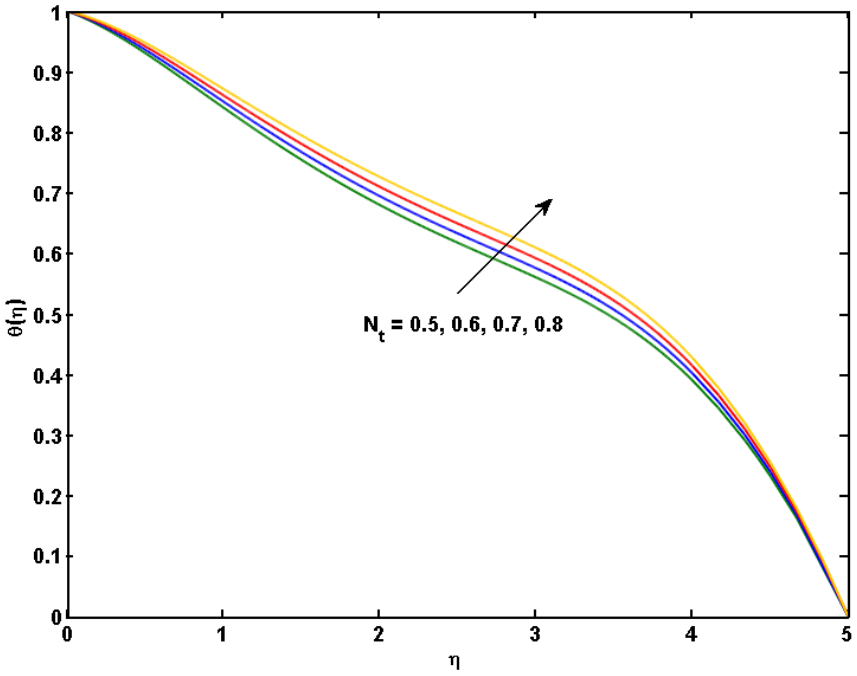

Fig.18 $\theta(\eta) Vs\ N_t$

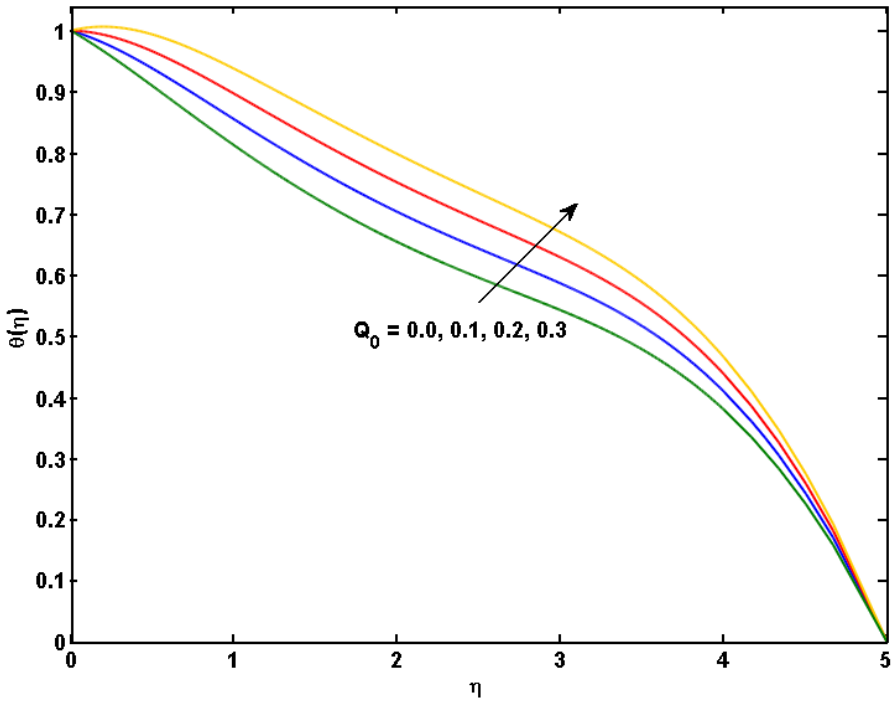

Fig.19 $\theta(\eta) Vs\ Q_0$

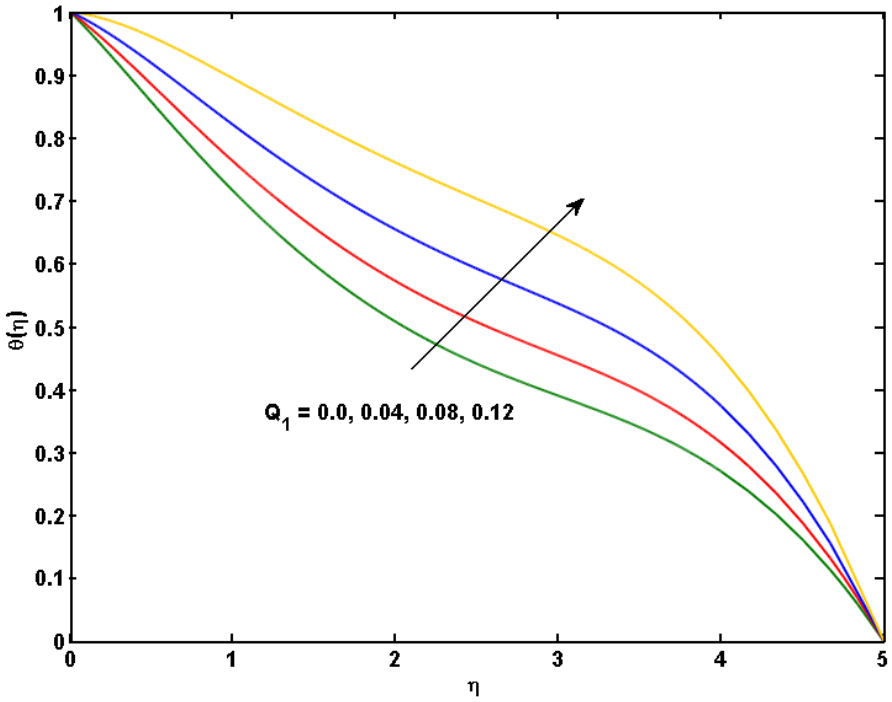

Fig.20 $\theta(\eta) Vs\ Q_1$

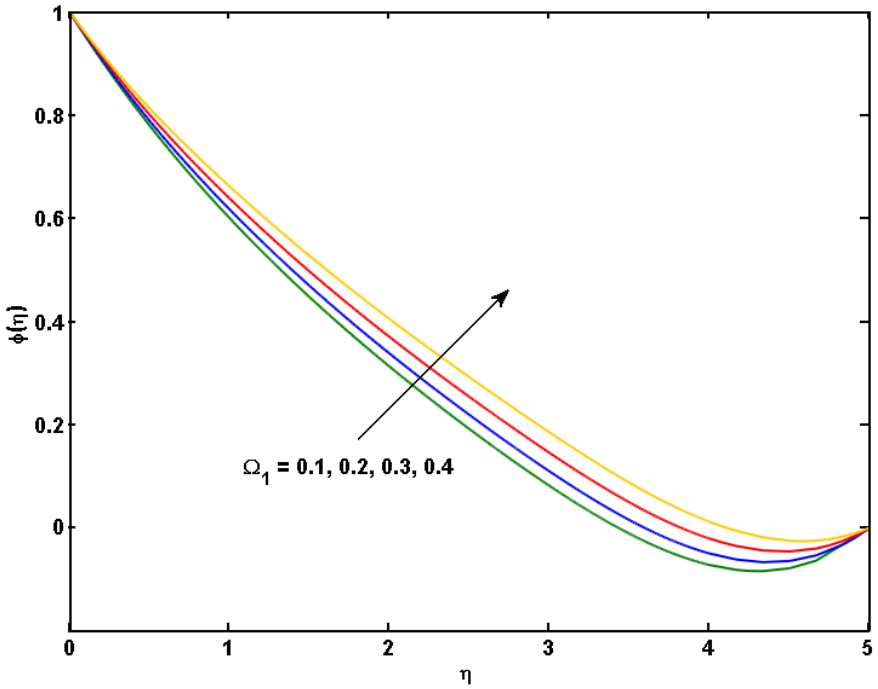

Fig.21 $\phi(\eta)$*Vs* Q_1

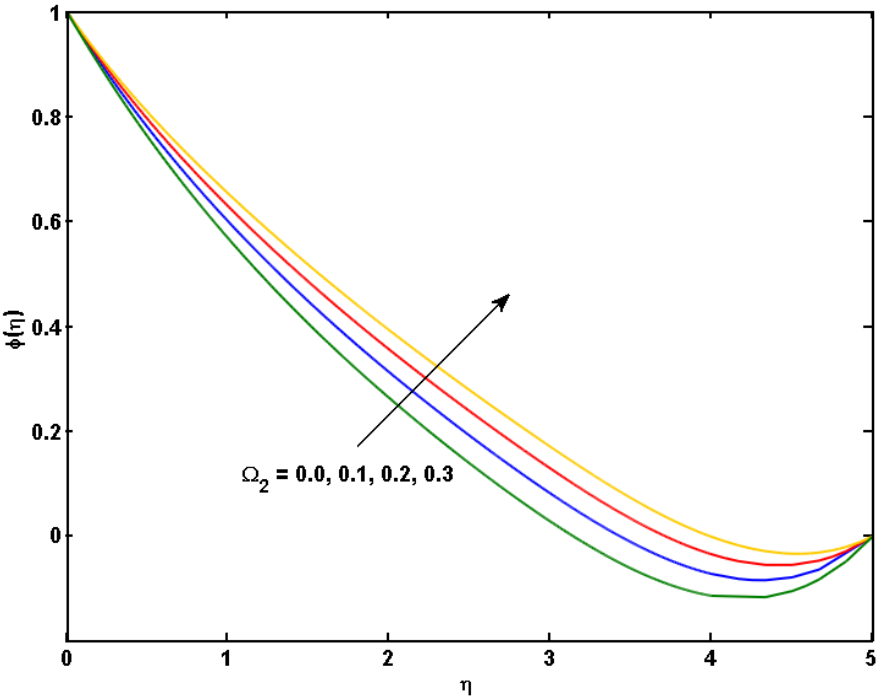

Fig.22 $\phi(\eta)$*Vs* Ω_2

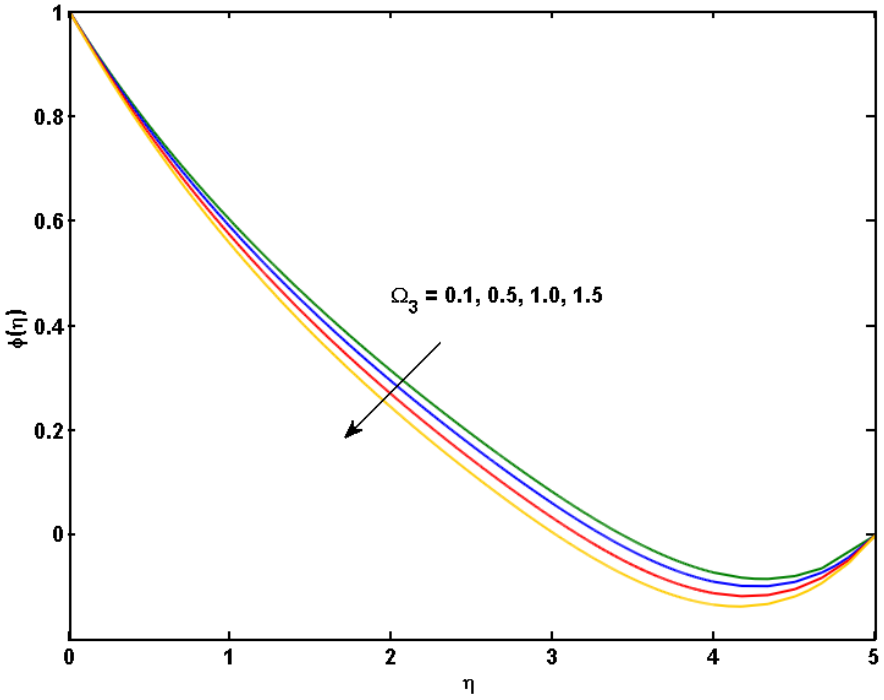

Fig.23 $\phi(\eta) Vs\ \Omega_3$

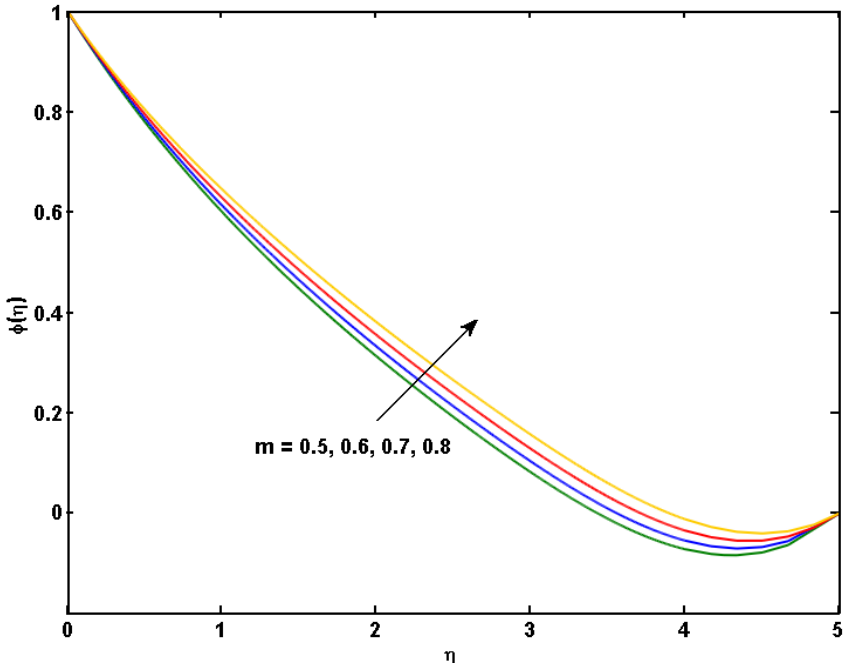

Fig.24 $\phi(\eta) Vs\ m$

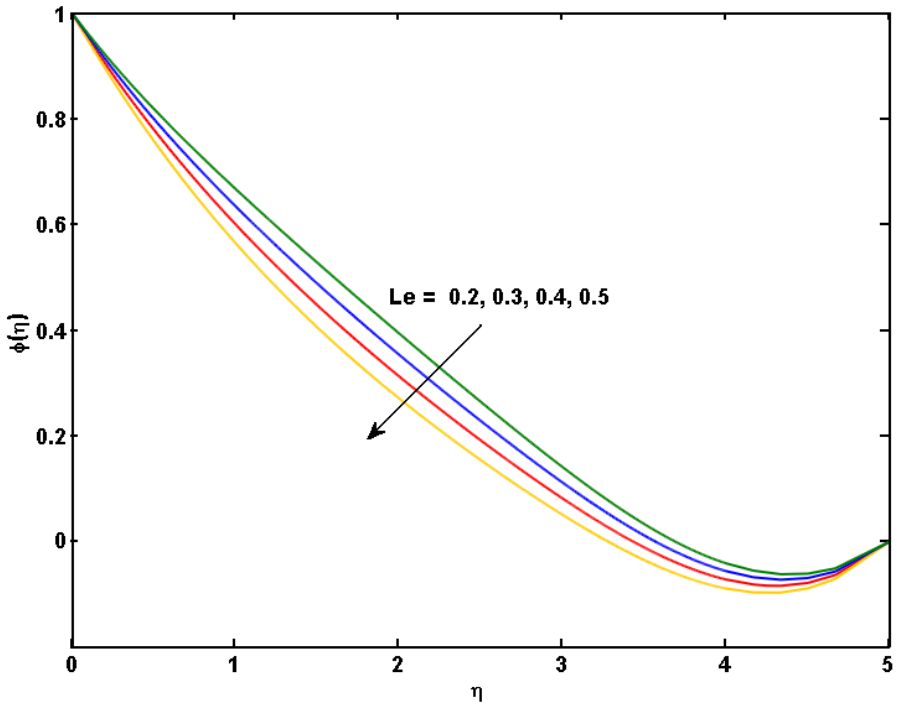

Fig.25 $\phi(\eta)$*Vs Le*

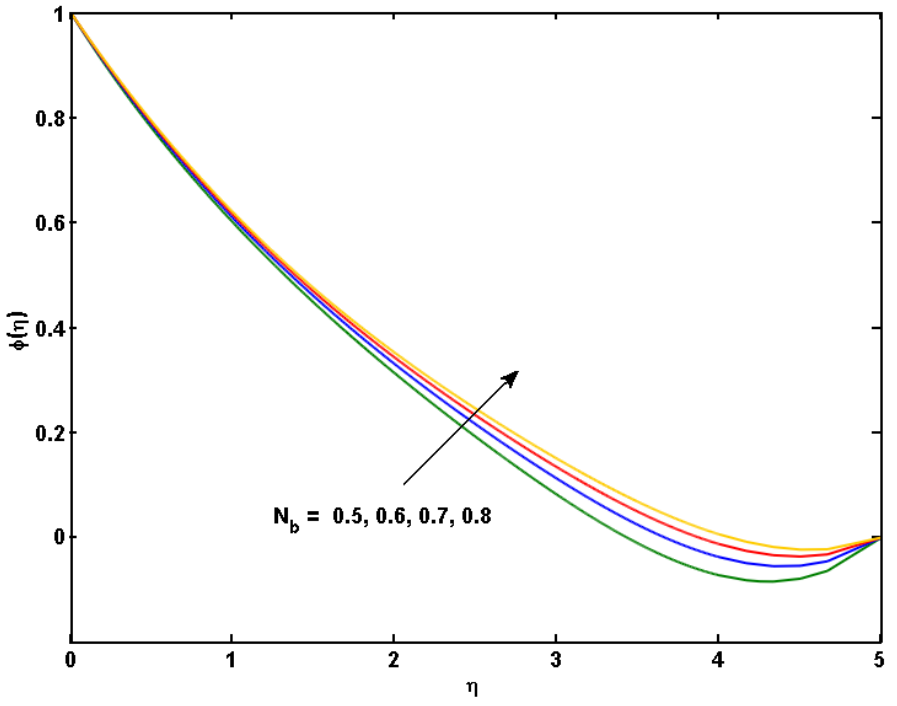

Fig.26 $\phi(\eta) Vs\ N_b$

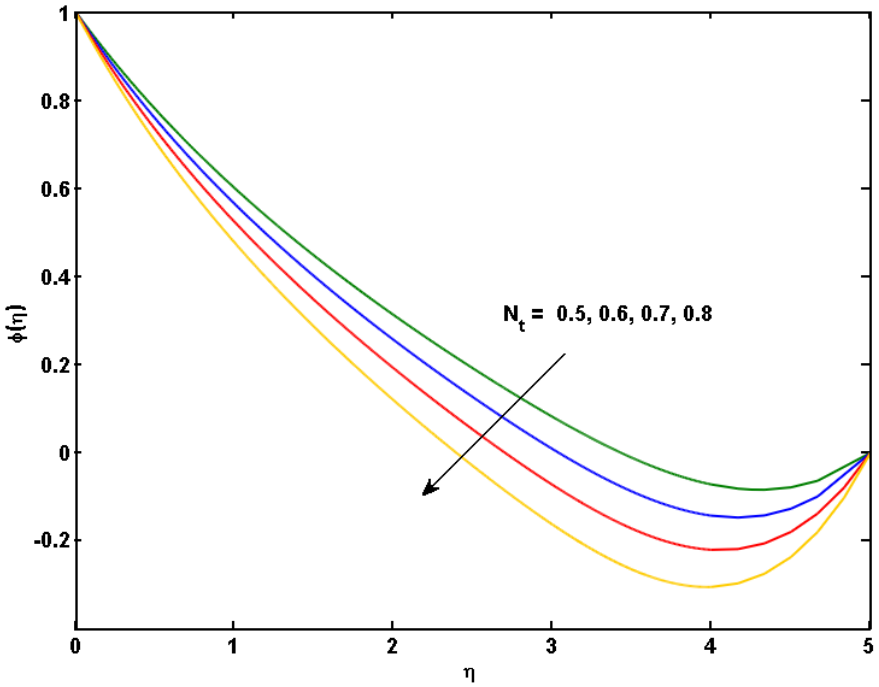

Fig.27 $\phi(\eta) Vs\ \ N_t$

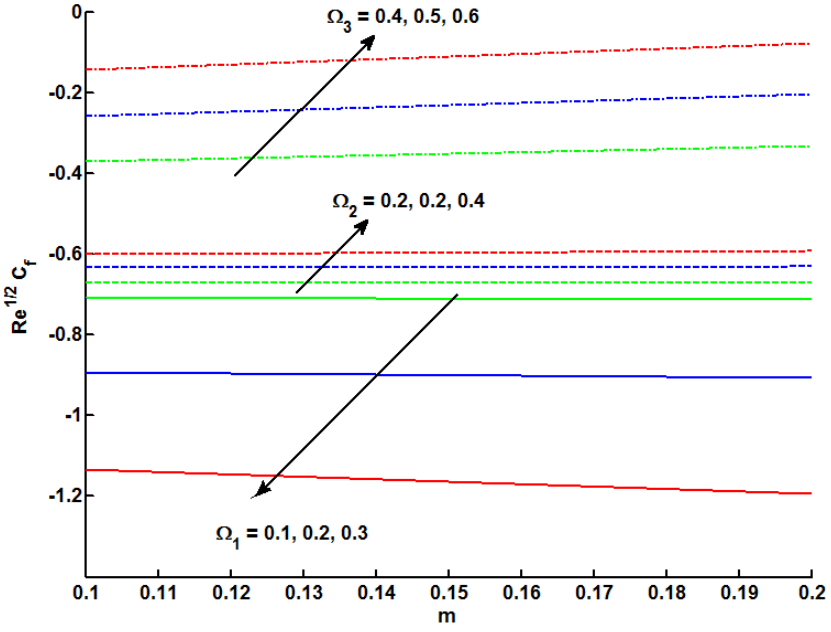

Fig.28. Effects of Ω_1, Ω_2 and Ω_3 on $\mathrm{Re}^{\frac{1}{2}} C_f$ against m

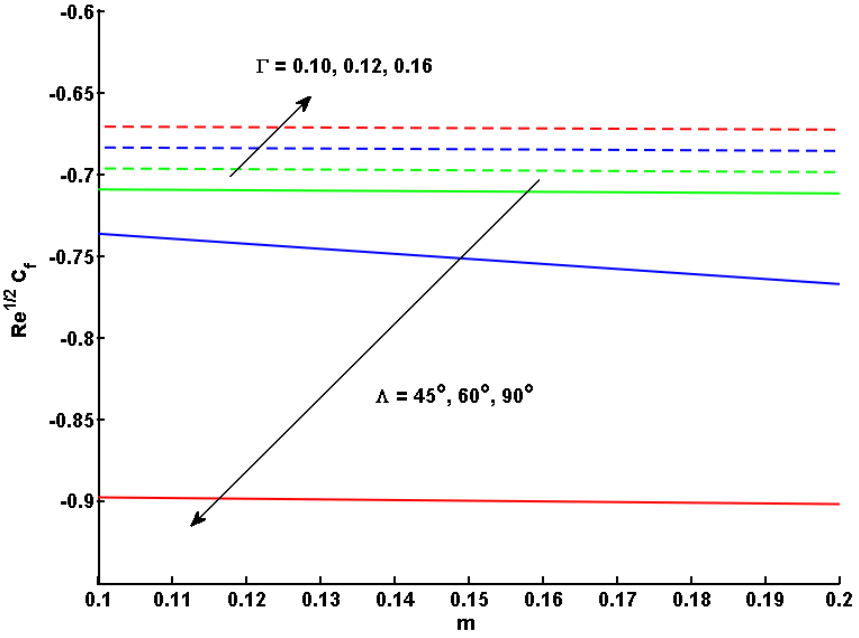

Fig.29. Effect of Λ and Γ on $\mathrm{Re}^{\frac{1}{2}} C_f$ against m

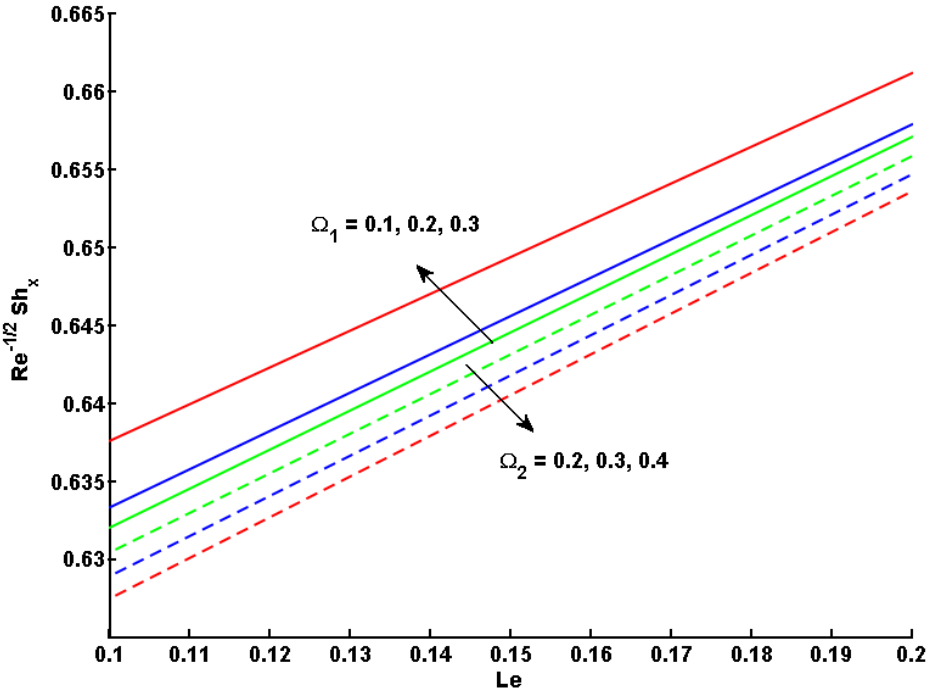

Fig.30. Effects of Ω_1 and Ω_2 on the Sherwood number against Le

5. Outcomes at a glance

The present study deals with the influence of non-uniform heat source/sink and temperature dependent viscosity on Cattaneo-Christov heat flow of third grade nanofluid past an inclined stretched Riga plate. The present investigation comes out with some important outcomes.

In the current analysis, accelerated fluid motion and thicker momentum boundary layers are due to increment in λ_T , λ_C , m , Γ . It has identified that increase in Ω_1 ascends the fluid motion while that of Ω_2 and Ω_3 exhibits reverse effect. It acknowledges that augmented Ω_1 and Ω_2 accounts for shrinkage of thermal boundary layer while that of Ω_3 establishes ascending thermal boundary layer. There are reports that enhanced N_b and N_t upsurges the fluid temperature while hike in Le belittles the fluid concentration leading to a descending concentration boundary layer. Further, increment in Q_0 and Q_1 contributes to increment in wall temperature gradient and yields an augmented wall shear stress. Finally, rise in Ω_1, Ω_2 and m has caused to upsurge the concentration while that of Ω_3 boils down it.

References

[1] S.U.S. Choi, Enhancing thermal conductivity of fluids with nanoparticles, ASME Fluids Eng. Division, 231 (1995) 99–105.

[2] L.G. Leal, Advanced Transport Phenomena: Fluid Mechanics and Convective Transport Processes. Cambridge University Press, New York (2007).

[3] W. A.. Khan, O. D Makinde, Z. H. Khan, Non-aligned MHD stagnation point flow of variable viscosity nanofluids past a stretching sheet with radiative heat. Int. J. Heat Mass Transf. 96 (2016) 525-534.

[4] M. I. Khan, T. Hayat, M. I. Khan, A. Alsaed, Activation energy impact in nonlinear radiative stagnation point flow of cross nanofluid. Int Comm. Heat Mass Transf 91(2018) 216–224.

[5] M. I. Khan, T. Hayat, A. Alsaed, Numerical investigation for entropy generation in hydromagnetic flow of fluid with variable properties and slip, Phys Fluid 30 (2018) 023601.

[6] M. I. Khan, M. Waqas, T. Hayat, A. Alsaed, Magneto-hydrodynamical numerical simulation of heat transfer in MHD stagnation point flow of Cross fluid model towards a stretched surface, Phys Chem Liq 56 (2018)584–595.

[7] M. Sheikholeslami, H. B. Rokni, CVFEM for effect of Lorentz forces on nanofluid flow in a porous complex shaped enclosure by means of non-equilibrium mode, J. Mol. Liq. 254 (2018) 446–462.

[8] M. Sheikholeslami, S. A. Shehzad, Simulation of water based nanofluid convective flow inside a porous enclosure via non-equilibrium model, Int. J. Heat Mass Transf. 120 (2018) 1200–1212.

[9] M. Sheikholeslami, M. Seyednezhad, Simulation of nanofluid flow and natural convection in a porous media under the influence of electric field using CVFEM, Int. J. Heat Mass Transf. 120 (2018) 772–781.

[10] M. K. Nayak, N. S. Akbar, V. S. Pandey, Z. H. Khan, D. Tripathi, 3D free convective MHD flow of nanofluid over permeable linear stretching sheet with thermal radiation, Powder Technol. 315 (2017) 205-215.

[11] M. K. Nayak, MHD 3D flow and heat transfer analysis of nanofluid by shrinking surface inspired by thermal radiation and viscous dissipation, Int. J. Mech. Sci. 124 (2017 185-193.

[12] M. K. Nayak, N. S. Akbar, V. S. Pandey, Z. H. Khan, D. Tripathi, MHD 3D free convective flow of nanofluid over an exponentially stretching sheet with chemical reaction, Adv. Powder Technol. 28(9) (2017) 2159-2166.

[13] M. K. Nayak, S. Shaw, V. S. Pandey, A. J. Chamkha, Combined effects of slip and convective boundary condition on MHD 3D stretched flow of nanofluid through porous media inspired by non-linear thermal radiation, Indian J Phys. 92(8) (2018) 1017-1028.

[14] A.S. Dogonchi, M. Waqas, D.D. Ganji, Shape effects of Copper-Oxide (CuO) nanoparticles to determine the heat transfer filled in a partially heated rhombus enclosure: CVFEM approach, Int. Comm. Heat Mass Transf. 107 (2019) 14-23.

[15] A.S. Dogonchi, M. Waqas, S.M. Seyyedi, M. Hashemi-Tilehnoee, D.D. Ganji, CVFEM analysis for Fe_3O_4-H_2O nanofluid in an annulus subject to thermal radiation, Int. J. Heat Mass Transf. 132 (2019) 473-483.

[16] A.S. Dogonchi, Ali J. Chamkha, M. Hashemi-Tilehnoee, S.M. Seyyedi, D.D. Ganji, Effects of homogeneous-heterogeneous reactions and thermal radiation on magneto-hydrodynamic Cu-water nanofluid flow over an expanding flat plate with non-uniform heat source, J. of Central South University26(5) (2019) 1161–1171.

[17] S.M. Seyyedi, N. Sahebi, A.S. Dogonchi, M. Hashemi-Tilehnoee, Numerical and experimental analysis of a rectangular single-phase natural circulation loop with asymmetric heater position, Int. J. Heat Mass Transf 130 (2019) 1343-1357.

[18] A.S. Dogonchi, D.D. Ganji, Effects of Cattaneo-Christov heat flux on buoyancy MHD nanofluid flow and heat transfer over a stretching sheet in the presence of Joule heating and thermal radiation impacts, Indian J. Phys. 92 757–766 (2018).

[19] F. Mabood, M. K. Nayak, A. J. Chamkha, Heat transfer on cross flow of micropolar fluids over a thin needle moving in a parallel stream influenced by binary chemical reaction and Arrhenius activation energy, European Physical J. Plus 134 (2019) 427.

[20] M. K. Nayak, R. Mehmood, O.D. Makinde, O. Mahian, Ali J. Chamkha, Magnetohydrodynamic flow and heat transfer impact on ZnO-SAE50 nanolubricant flow due to an inclined rotating disk, J. Central South University 26 (2019) 1146-1160.

[21] M. K. Nayak, Sachin Shaw, Ali J Chamkha, MHD free convective stretched flow of a radiative nanofluid insprired by variable magnetic field, Arabian J. Sci. Engi. 44(2) (2019) 1269-1282.

[22] M. K. Nayak, I. S. Oyelakin, S. Mondal, S.S. Sen, Impact of the Cattaneo ‐ Christov thermal and solutal diffusion models on the stagnation point slip flow of Walters' B nanofluid past an electromagnetic sheet, Heat Transf. Asian Res. 48(2) (2019) 713-726.

[23] A. Pantokratoras, E. Magyari, MHD free-convection boundary-layer flow from a Riga-plate. J *Eng. Math*. 64 (2009) 303-315.

[24] A. Ahmad, S. Asghar, S. Afzal, Flow of nanofluid past a Riga plate. *J.Magn. Magn. Mat*. 402 (2016) 44–48.

[25] A.K. Abdul Hakeem, M. K. Nayak, O. D. Makinde, Effect of exponentially variable viscosity and permeability on Blasius flow of Carreu nanofluid over an electromagnetic plate through a porous medium, J. Appl. Computational Mech. 5(2) (2019) 390-401.

[26] T. Hayat, A. Kiran., M. Imtiaz, A. Alsaedi, M. Ayub, Melting heat transfer in the MHD flow of a third-grade fluid over a variable-thickness surface. *Eur. Phys. J. Plus.* 132 (2017) 265.

[27] G. J. Reddy, A. Hiremath, M. Kumar, Computational modeling of unsteady third-grade fluid flow over a vertical cylinder: A study of heat transfer visualization. *Results in Phys*.8 (2018) 671–682.

[28] C. Cattaneo, C. D. C. Sulla, Atti Sem. *Mat. Fis. Univ. Modena*.3(1948) 83–101.

[29] C. I. Christov, On frame indifferent formulation of the Maxwell-Cattaneo model of finite-speed heat conduction, Mech Res Commun.36(4) (2009) 481–6.

[30] M. Imtiaz, A. Alsaedi, A. Shafiq, T. Hayat, Impact of chemical reaction on third grade fluid flow with Cattaneo-Christov heat flux, J.of Mol. Liq. 229 (2017) 501–507.

[31] T. Hayat, S. Nadeem, Flow of 3D Eyring-Powell fluid by utilizing Cattaneo-Christov heat flux model and chemical processes over an exponentially stretching surface, Results in Phys. 8 (2018) 397–403.

[32] P. R. Sharma, S. Sinha, R. S. Yadav, A. N. Filippov, MHD mixed convective stagnation point flow along a vertical stretching sheet with heat source/sink, Int. J. of Heat and Mass Transf. 117(2018) 780–786.

[33] E. Grinberg, On determination of properties of some potential fields, Appl Magnetohydrodyn. Rep Phys Inst Riga 12 (1961) 147–154.